Crystal Structure, Electrical Transport, and Magnetic Properties of Niobium Monophosphide

J. Xu, M. Greenblatt,* T. Emge, and P. Höhn

Department of Chemistry, Rutgers, The State University of New Jersey, Piscataway, New Jersey 08855-0939

T. Hughbanks* and Y. Tian

Department of Chemistry, Texas A & M University, College Station, Texas 77843-3255

Received July 7, 1995[⊗]

Large single crystals of NbP have been prepared. A single-crystal X-ray diffraction study shows that it crystallizes in tetragonal symmetry with space group $I4_1md$ (No. 109) and lattice parameters $a = 3.3324(2)$ Å, $c = 11.3705(7)$ Å, and $Z = 4$. A full matrix least-squares refinement based on a unique data set of 285 reflections ($I > 2\sigma(I)$) yielded $R(F) = 0.017$ and $R_w(F^2) = 0.046$ for nine variables. The unit cell consists of one unique Nb and one P, each in trigonal prismatic coordination with the other element. There are two short and four long bond distances of Nb−P. The Nb−Nb bond distances are significantly shorter than $R_c = 4.09$ Å, the critical distance required for good Nb−Nb 4d orbital overlap for niobium metal−metal bonds. NbP shows metallic behavior with $\rho = 4.5 \times 10^{-5}$ Ω cm at room temperature. Magnetic susceptibility measurements on a collection of randomly oriented single crystals indicate very weak Pauli paramagnetism ($\sim 10^{-5}$ emu/mol). A discussion of the structure as well as the physical properties of NbP compared with those of previous results are presented. The band structure of NbP based on the extended Hückel (tight-binding) calculations is presented along with an analysis that reveals that the valence band is built up from three center bonds localized within Nb_3 triangles.

Introduction

A number of investigators have prepared polycrystalline niobium monophosphide by solid state reaction methods and investigated its properties by chemical analysis, powder X-ray diffraction, NMR, magnetic susceptibility, and electrical transport measurements. The structure of NbP has been studied: first by Schönberg[1] in 1954, followed by Boller and Parthe,[2] Furuse and Kjekshus,[3] and finally Willerstrom in 1984.[4] On the basis of powder X-ray diffraction analysis, it appears that NbP is isostructural with NbAs.[2] The electrical resistivity as a function of temperature reported by Ripley[5] indicated that NbP was a metallic conductor with room temperature resistivity $\sim 10^{-2}-10^{-3}$ Ω cm. However, magnetic susceptibility reported by Scott *et al.*[6] showed that NbP was diamagnetic with a small orbital Knight shift, which suggested a near zero band gap.

In order to clarify some of the controversy in the previously reported data, we had three major objectives: (1) to carry out a single-crystal X-ray structure analysis to determine accurate bond distances and angles (2) to obtain oriented single-crystal resistivity measurements on NbP, since prior resistivity measurements were made on polycrystalline pellets,[5] and (3) to clarify the relationship between structure and electrical transport and magnetic properties, as well as to construct a schematic band diagram.

* To whom correspondence should be addressed.

[⊗] Abstract published in *Advance ACS Abstracts,* January 15, 1996.

(1) Schönberg, N. *Acta Chem. Scand.* **1954**, *8*, 226.
(2) Boller, H.; Parthe, H. *Acta Crystallogr.* **1963**, *16*, 1095.
(3) Furuseth, S.; Kjekshus, A. *Acta Crystallogr.* **1964**, *17*, 1077.
(4) Willerstrom, J.-O. *J. Less-Common Met.* **1984**, *99*, 273.
(5) Ripley, R. L. *J. Less-Common Met.* **1962**, *4*, 496.
(6) Scott, B. A.; Eulenberger, G. R.; Bernheim, R. A. *J. Chem. Phys.* **1968**, *48*, *1*, 263.
(7) Fair, C. K. MOLEN, Enraf-Nonius, Delft Instruments X-Ray Diffraction B. V., Rontgenweg 1, 2624BD Delft, The Netherlands, 1990.

Experimental Section

Sample Preparation. During an investigation of the La−Nb−P−O system, shiny, silver single crystals of unknown composition were obtained as a result of a chemical vapor transport reaction. The synthetic procedure was performed in two steps. A reaction mixture containing $La_2(C_2O_4)_3 \cdot 10H_2O$ (Alfa, 99.99%), Nb_2O_5 (Alfa, 99.5%), and $(NH_4)_2HPO_4$ (Fisher, 99.7%) in a molar ratio of 1.5:2.3:4 was ground in an agate mortar and heated at 600 °C in a porcelain crucible for 4 h to decompose $La_2(C_2O_4)_3 \cdot 10H_2O$ and $(NH_4)_2HPO_4$ and to remove CO_2, H_2O, and NH_3. The decomposition temperature of the mixture was determined by TGA. The resulting powder was then mixed with the required amount of niobium metal powder (Johnson Matthey Electronics, 99.8%) to achieve a composition of $La_3Nb_6P_4O_{26}$. NH_4Cl (5 mol%) was added as chemical transport agent. The mixture was pelletized and sealed in an evacuated ($\sim 10^{-6}$ Torr) quartz tube. The quartz tube was placed horizontally inside a muffle furnace and heated at 1250 °C for a week, and then it was slowly cooled (5 °C/h) to 900 °C, followed by 50 °C/h to 500 °C and then quenched to room temperature. La_2O_3 white powder was observed in the hot end, while shiny silver crystals, subsequently determined to be NbP, deposited in the cool end of the quartz tube.

Single-Crystal X-ray Diffraction Data. A single crystal of NbP with dimensions $0.040 \times 0.076 \times 0.078$ mm^3 was mounted approximately along the *a* axis. The data were collected on an Enraf-Nonius CAD4 diffractometer with graphite monochromatized Mo Kα radiation at room temperature. The 1179 intensity data points were measured up to $\theta = 45°$ with ω scans. The unit cell parameters were determined by the least-squares fit of 25 peaks with $20.0 < 2\theta \leq 33.1°$. Of the 306 independent reflections, 285 had $I > 2\sigma(I)$. The intensity of three standard reflections varied less than 1% during the data collection. The data were corrected for Lorentz effects (polarization and extinction); absorption corrections were performed based on a ψ-scan (MOLEN).[7] The cell parameters and detailed setting of data collection are given in Table 1.

Determination and Refinement of the Structure. Shelxs-86[8] (direct methods) and Shelxl-93[9] packages were used for the crystal structure solution and refinement, respectively. The general reflection

0020-1669/96/1335-0845$12.00/0

Table 1. Crystallographic Data for NbP

formula	NbP
fw	123.88
space group (No.)	$I4_1md$ (109)
temp, °C	20
a, Å	3.3324(2)
c, Å	11.3705(9)
Z	4
V, Å^3	126.29(1)
ρ_{calcd}, g cm^{-3}	6.52
λ, Å	0.71073
μ, cm^{-1}	99.5
min/max values of absorption correction	86.18/99.81
$R(I > 0)$[a]	0.021 on F for 306 reflections
$R(I > 2\sigma(I))$[a]	0.017 on F for 285 reflections
R_w[a]	0.042 on F^2 for 306 reflections

[a] $R(F) = \sum||F_o| - |F_c||/\sum|F_o|$. $R_W(F^2) = \{\sum[w(F_o^2 - F_c^2)^2]/\sum[w(F_o^2)^2]\}^{1/2}$.

Table 2. Atomic Fractional Coordinates and Equivalent Isotropic Displacement Coeffients (Å^2) for NbP[a]

element	x	y	z	U_{equiv}[b]
Nb	0	0	0	0.0034(1)
P	0	0	0.41737(9)	0.0043(1)

[a] Estimated standard deviations of refined parameters are enclosed in parentheses. [b] $U_{(equiv)} = {}^1/_3(U_{11} + U_{22} + U_{33})$.

Table 3. Bond Distances (Å) and Bond Angles (deg) for NbP[a]

Nb−P	2.5294(7) × 2
Nb−P	2.5368(4) × 4
Nb−Nb	3.2950(2) × 4
Nb−Nb	3.3324(2) × 4
P(i)−Nb−P(ii)[b]	82.41(3)
P(i)−Nb−P(iv)	81.141(7)
P(ii−Nb−P(iv)	135.34(2)
P(iii)−Nb−P(v)	82.11(1)
P(v)−Nb−P(vi)	136.52(4)

[a] Estimated standard deviations are enclosed in parentheses. [b] Symmetry code: (i) $-y + {}^1/_2, x, z - {}^1/_4$; (ii) $-y - {}^1/_2, x, z - {}^1/_4$; (iii) $x - {}^1/_2, y - {}^1/_2, z - {}^1/_2$; (iv) $x + {}^1/_2, y + {}^1/_2, z - {}^1/_2$; (v) $x - {}^1/_2, y + {}^1/_2, z - {}^1/_2$; (vi) $x + {}^1/_2, y - {}^1/_2, z - {}^1/_2$.

conditions ($h + k + l = 2n$ for hkl, $h + k = 2n$ for $hk0$, $k + l = 2n$ for $0kl$ and $2h + l = 4n$; $l = 2n$ for hhl, $l = 4n$ for $00l$, $k = 2n$ for $0k0$, and $h = 2n$ for $hh0$) led to possible space groups $I4_1md$ (No. 109) and $I42d$ (No. 122). The structure was solved and refined successfully in the space group $I4_1md$. The structure and thermal parameters refined by full-matrix least-squares methods led to $R(F) = 0.021$ and $R_w(F^2) = 0.042$ for all data. The maximum and minimum residual electron densities in the final difference Fourier map were 0.80 e/Å^3 near the P atom at (0,−0.5,0.4165) and −2.44 e/Å^3 close to Nb at (0,0,0.0487). The final atomic and thermal parameters are given in Table 2. Table 3 contains the bond distances and bond angles.

Electrical Transport and Magnetic Susceptibility Measurements. Electrical resistivity measurements on a single crystal of NbP (∼1.6 × 0.4 × 0.4 mm^3) were made by a standard four-probe technique with a Displex Cryostat (APD cryogenics, model DE 202) in the temperature range 30−300 K. Copper leads and silver paint were used to make ohmic contacts to the sample. The I−V profiles were recorded at different temperatures to ensure the ohmic nature of the contacts. There was no appreciable variation of the resistivity between cooling and heating cycles.

Magnetic susceptibility data on a collection of randomly oriented single crystals of NbP (18.1 mg) were recorded with a Quantum Design SQUID magnetometer in the temperature range 2−300 K. The applied magnetic field was 0.5 T. The susceptibility data were corrected for the core diamagnetic contributions of the component ions.

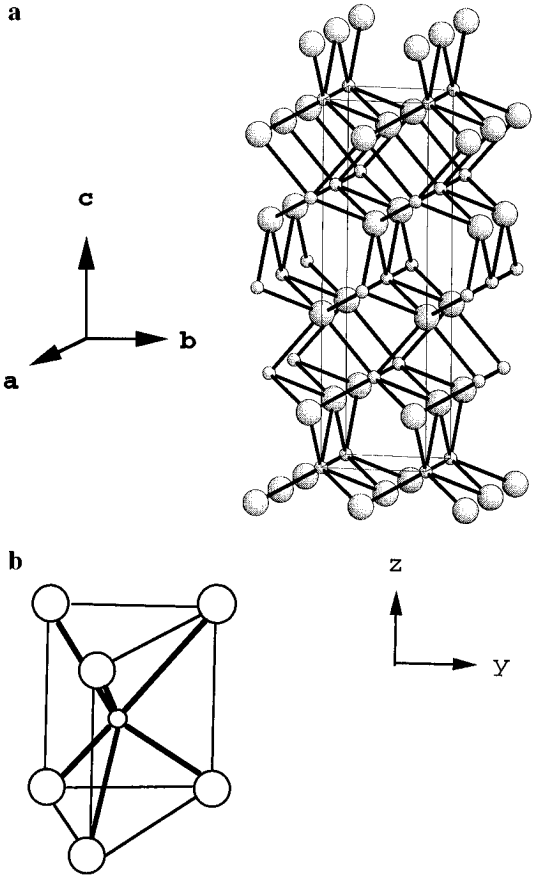

Figure 1. (a) Projection of NbP on *ac* plane. (b) One trigonal prism unit. Large circle is P, and small circle is Nb.

Results and Discussion

Synthesis. Relatively large crystals of NbP were obtained in an attempt to prepare a polycrystalline sample of $La_3Nb_6P_4O_{26}$ from a stoichiometric mixture of the constituent starting materials. Subsequently our attempts to grow the single crystals without $La_2(C_2O_4)_3{\cdot}10H_2O$ in the initial reaction mixture led to microcrystals (∼10 μm) which are inappropriate for physical measurement. Thus La_2O_3 serves in some, yet undetermined, way to promote the growth of large NbP crystals.

Description of the Structure. The single-crystal study confirms the structural model which had been previously proposed from X-ray powder data for β-NbP.[2] However, the atomic positions have been determined with higher accuracy by the single-crystal X-ray analysis.

The projection of the structure of NbP on the *ac* plane is shown in Figure 1. The structure is built up of NbP_6 and PNb_6 trigonal prisms. These NbP_6 (or PNb_6) trigonal prisms are extended on the *ab* plane and stacked along the *c* axis by the 4-fold screw axis. Alternatively, each *ab* plane is formed by a sheet of Nb atoms which is separated by a sheet of P atoms.

On the basis of their X-ray powder diffraction data, Boller and Parthe[2] reported that the Nb−P bond distance is 2.54(0) Å. The Nb−P bond distances obtained in our refinement are normal for trigonal prismatic coordinated (NbP_6/PNb_6) niobium phosphides.[10,11] The local trigonal prismatic environments in NbP are only slightly distorted, with two short (2.5294(7) Å)

(8) Sheldrick, G. M. *Shelxs-86*; Universität Göttingen: Göttingen, FRG, 1986.
(9) Sheldrick, G. M. *Shelxl-93*; Universität Göttingen, Göttingen, FRG, 1993.
(10) Hassler, E. *Acta Chem. Scand.* **1971**, *25*, 129.
(11) Anugul, S.; Pontchour, C.; Rundavist, S. *Acta Chem. Scand.* **1973**, *27*, 26.

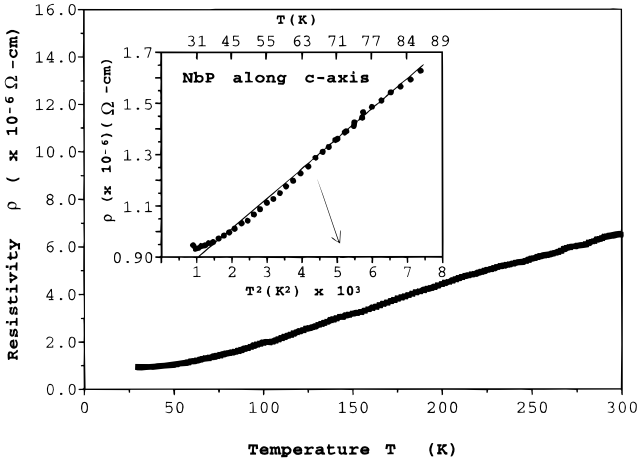

Figure 2. Resistivity as a function of temperature of NbP along the *c* axis crystallographic direction.

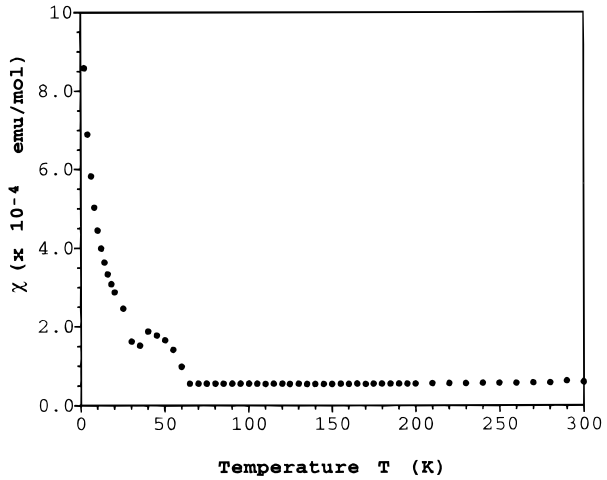

Figure 3. Magnetic susceptibility as a function of temperature on a batch of unoriented single crystals of NbP.

and four longer (2.5368(4) Å) Nb−P distances. The symmetry of the distorted trigonal prisms of NbP_6/PNb_6 is C_{2v}.

The niobium metal−metal bond distances are considerably longer than that of 2.8 Å in niobium metal and 2.6 Å found in niobium cluster compounds such as $Ca_{0.75}Nb_3O_6$.[12] The Nb−Nb separation in the *ab* plane of NbP is 3.3324(2) Å, while between the planes it is slightly shorter, 3.2950(2) Å. These distances allow for modest, but significant, metal−metal interaction between niobium atoms in NbP. Both in-plane (*ab*) and between-plane distances are smaller than the critical distance ($R = 4.09$ Å) for good overlap of the 4d orbitals of Nb in NbP.[6]

Electrical Transport and Magnetic Properties. NbP was reported to be metallic with a room temperature specific resistivity of 1.7×10^{-3} Ω/cm.[5] Electrical resistivity measurements along the *c* axis of a single crystal indicate that the room temperature resistivity is 4.5×10^{-5} Ω cm, which is comparable with that of highly metallic NbAs (7.0×10^{-5} Ω cm).[13] The electrical resistivity as a function of temperature along the *c* axis (Figure 2) decreases linearly with decreasing temperature down to ∼100 K. This is typical of metallic behavior. Below 100 K, the slightly nonlinear behavior of resistivity as a function of *T* is linear as a function of T^2 (see inset of Figure 2). This behavior is generally attributed to electron scattering. The resistivity in the *ab* plane is about 1 order of magnitude smaller than that along the *c* axis. This will be further discussed below. NbP can be formulated as $Nb^{3+}P^{3-}$; thus the $4d^2$ electrons of Nb^{3+} partially fill a conduction band, which results in metallic behavior. Seebeck measurements indicate n-type conductivity, consistent with electrons being the majority carriers.

The magnetic susceptibility measurement shows temperature independent Pauli paramagnetic behavior from 65 to 300 K with an average slightly negative magnetic susceptibility of -16.9×10^{-6} emu/mol. After correcting for the core diamagnetism of -24×10^{-6} emu/mol for Nb^{3+} and -50×10^{-6} emu/mol for P^{3-},[14] we obtained $\chi = 61 \times 10^{-6}$ emu/mol for NbP at room temperature. Figure 3 shows the magnetic susceptibility as a function of temperature. A small peak around 50 K arises from the antiferromagnetic ordering of absorbed O_2.[15] The upturn below 50 K is due to small magnetic impurities in the sample.

Bonding and Electronic Structure Many years ago, Scott *et al*. proposed a schematic band diagram for NbP that accounted for their finding that NbP was diamagnetic.[6] The band structure

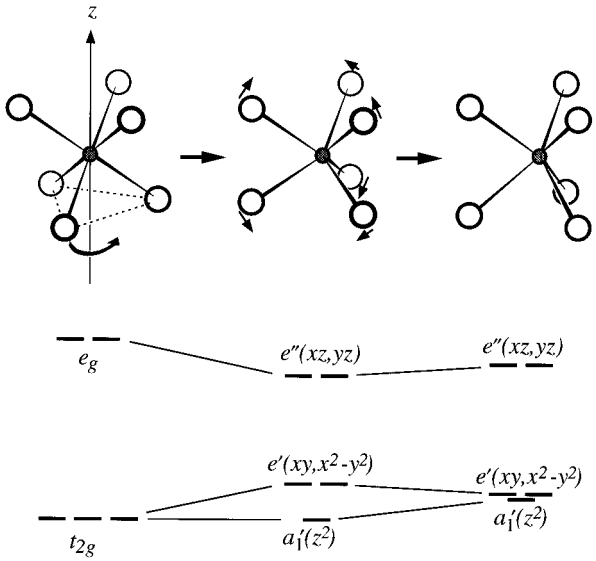

Figure 4. Schematic correlation diagram for the d orbital splitting induced by an octahedron and a trigonal prism; the latter is derived from the former by a turnstile rotation of a ML_3 unit. When the ligands are equidistant from each other the $a_1' - e'$ splitting is small (at right).

they proposed suggested that NbP was a small-band-gap semiconductor. In view of the metallic conductivity and Pauli paramagnetism we have observed in the present investigation, it was deemed necessary to revisit the band structure of NbP.

As we have discussed, the NbP_6 trigonal prisms in NbP show very little deviation from ideal local D_{3h} symmetry; all Nb−P distances fall within 0.004 Å of 2.533 Å, and all Nb−P bonds fall within 0.2° of a cone that makes a 48.9° angle to the prisms pseudo-3-fold axis. Furthermore, all the P−P contacts in the trigonal prisms are also of very nearly equal length, within 0.015 Å of 3.310 Å. Because the details of the Nb local coordination environment are important in understanding the effective ligand-field splitting that the Nb 4d levels experience, it is instructive to compare the trigonal prismatic NbP_6 environment in NbP with an octahedron. In Figure 4 we show a qualitative correlation diagram (derived from an angular overlap model with Nb−P σ interactions only) in which a trigonal prism is obtained from an octahedron by first twisting one triangular face by 60° about a 3-fold axis and then relaxing the prism angles so that all the atoms at the prism vertices are equidistant. In the first

(12) Hibble, S. J.; Cheetham, A. K.; Cox, D. E. *Inorg. Chem.* **1987**, *26*, 2389.
(13) Schafer, H.; Fuhr, W. *J. Less-Common Met*. **1965**, *8*, 375.
(14) Jeitschko, W.; Reehuis, M. *J. Phys. Chem. Solids* **1987**, *48*, *7*, 667.
(15) Quantum Design Technical Advisory MPMS No. 8; Quantum Design, Inc., 1990.

Chart 1

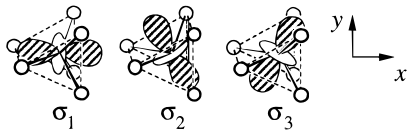

1

Chart 2

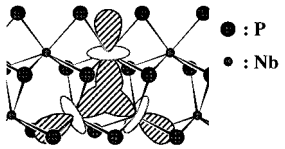

2

step of this process, the nonbonding t_{2g} d orbitals are split such that one remains nonbonding (z^2, if the z axis is taken along a 3-fold axis) and two (x^2-y^2 and xy) acquire some metal−ligand antibonding character and are pushed up in energy. The $a_1'(z^2)$ orbital remains nonbonding because the ligands lie in the z^2 orbital node during the turnstile motion in this step. In the second step, the z^2 orbital is destabilized as the ligands are moved out of the node and some overlap develops; at the same time the $e'(x^2-y^2$ and $xy)$ set is stabilized as the ligands move away from the xy plane and the orbitals' overlap with ligand orbitals is decreased. The net result is that the splitting between the $a_1'(z^2)$ orbital and the $e'(x^2-y^2$ and $xy)$ orbitals is quite small.

The near degeneracy of the $a_1'(z^2)$ orbital and the $e'(x^2-y^2$ and $xy)$ orbitals is often not appreciated in considering materials where trigonal prismatic metal coordination is involved. It means that if there are perturbations to these levels which are much greater in magnitude than the z^2 − (x^2-y^2, xy) orbital splitting, then this splitting can be neglected when we treat the effects of such perturbations. Specifically, if we wish to consider the interaction of the central metal with atoms that interact through the square faces of the prism, then the strength of that interaction will be much more important than the small gap that separates the z^2 and (x^2-y^2, xy) orbitals. This is the usual case for trigonal prism geometries encountered in solid state structures.

Because of the near degeneracy between the $a'(z^2)$ and the $e'(x^2-y^2$ and $xy)$ orbitals, it is quite convenient to consider a symmetrical alternative set of d orbitals, (σ_1, σ_2, σ_3), that are constructed as linear combinations of the z^2 and (x^2-y^2, xy) orbitals:[16,17]

$$\sigma_1 = \frac{-1}{\sqrt{3}}d_{z^2} + \sqrt{\frac{2}{3}}d_{x^2-y^2}$$

$$\sigma_2 = \frac{-1}{\sqrt{3}}d_{z^2} - \frac{1}{\sqrt{6}}d_{x^2-y^2} - \frac{1}{\sqrt{2}}d_{xy} \qquad (1)$$

$$\sigma_3 = \frac{-1}{\sqrt{3}}d_{z^2} - \frac{1}{\sqrt{6}}d_{x^2-y^2} + \frac{1}{\sqrt{2}}d_{xy}$$

These orbitals are depicted schematically in Chart 1; each resembles a "z^2-like" orbital that is well-directed for σ overlap through one of the square prism faces with orbitals centered on nearby atoms. When the NbP structure is pieced together using these building blocks, each Nb is found to participate in the formation of three distinct 3c−2e bonds; this process is depicted in Chart 2 for one such 3c−2e bond. The strength of this bonding depends on the Nb−Nb distances, and it is useful to compare explicitly calculated results with the qualitative description so far discussed. In Figure 5, we show a density of states (DOS) diagram obtained from an extended Hückel calculation on NbP; parameters and other computational details concerning the calculation are given in the Appendix. The first panel in the figure shows the total DOS, along with a curve showing the niobium contribution. The Fermi level lies in a deep minimum in the DOS; there is only a modest overlap between the valence and conduction bands. This is consistent with the metallic properties and the small Pauli paramagnetism ($\sim 10^{-5}$ emu/mol) we have observed. In the second panel, separate curves indicate contributions for the orbitals corresponding to the metal a_1' and e' orbitals; it is clear that there is a large overlap in the energetic distribution of the a_1' and e' contributions and that both orbital contributions span the Fermi level. However, when we project a linear combination of orbitals corresponding to the three-center bond orbitals depicted in Chart 2 (right panel in Figure 5), we see that the occupied portion of the d bands clearly has the three-center-bonding character we have described.

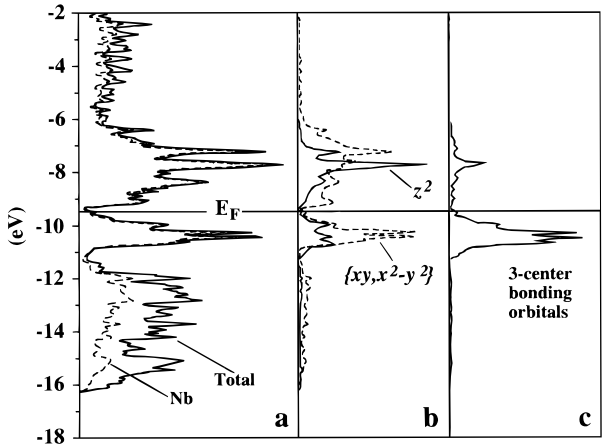

Figure 5. DOS (density of states) for NbP. (a) Total DOS for NbP (solid line) and projected DOS for Nb contribution (dashed line); levels shown span the Nb 4d and P 3p band regions. (b) Nb d_{z^2} (solid line) and ($d_{x^2-y^2}$, d_{xy}) (dashed line) projections. (c) Three-center-bonding orbital projection.

The exposition given above closely follows the description we have previously provided for other materials built with trigonal prismatic building blocks: MoS_2, LnI_2 (Ln = La, Ce, Pr, Gd), Pr_2X_5 (X = Br, I), and WC-type ZrS.[16,17] The relationship between NbP and ZrS is particularly close. They are isoelectronic compounds with three-dimensional network structures and have very similar electronic structures in which a metallic state is found to result from a small overlap of three-center-bonding and three-center-antibonding bands. The metallic state found for ZrS and NbP arises from interactions that widen both the valence and conduction bands enough to cause the valence−conduction band overlap. In both instances, these are interactions between three-center bond orbitals that are absent in the layered compounds (MoS_2-type) and chain compounds (Pr_2X_5). The three-center bonding discussion above accounts for six out of eight total Nb−Nb contacts surrounding each metal center (each metal is involved in three distinct three-center bonds). However, there are z^2-z^2 overlaps of the type illustrated in Chart 3 with two additional neighbors. These interactions cause valence and conduction band dispersion to be greater in the *ab* plane for NbP and up the *c* axis in ZrS. Thus we expect greater conductivity in the *ab* plane for NbP

(16) Yee, K. A.; Hughbanks, T. *Inorg. Chem.* **1991**, *30*, 2321.
(17) Tian, Y.; Hughbanks, T. *Inorg. Chem.* **1993**, *32*, 400.

Chart 3

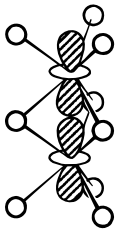

3

(as we have observed) and greater conductivity parallel to the *c* axis for ZrS (which, to our knowledge, has not been measured).

Conclusion

NbP crystallizes in a tetragonal system and consists of a network of slightly distorted NbP_6 and PNb_6 trigonal prisms. The fusion of the NbP_6 prisms allows for moderate Nb 4d orbital overlap that results in the formation of three-center two-electron bonding within Nb_3 triangles. The interaction between these otherwise localized three-center bonds results in a metallic state and anisotropic conductivity wherein conductivity is greater in the *ab* planes. There is only a small valence−conduction band overlap that gives rise to a weak Pauli paramagnetism.

Acknowledgment. We thank Professors W. H. McCarroll and K. V. Ramanujachary for critically reading this manuscript and for their useful comments. Research at Rutgers was supported by the National Science Foundation Solid State Chemistry Grant DMR-93-14605. Research at Texas A & M was generously supported by the National Science Foundation through Grant DMR-9215890.

(18) Whangbo, M.-H.; Evain, M.; Hughbanks, T.; Kertesz, M.; Wijeyesekera, S.; Wilker, C.; Zheng, C.; Hoffmann, R. *EHMACC: Extended Hückel Molecular and Crystal Calculations*; Whangbo, M.-H., Evain, M., Hughbanks, T., Kertesz, M., Wijeyesekera, S., Wilker, C., Zheng, C., Hoffmann, R., Eds.; Quantum Chemistry Program Exchange: 9, 61, 1989.
(19) Hoffmann, R. *J. Chem. Phys.* **1963**, *39*, 1397.
(20) Clementi, E.; Roetti, C. *At. Nucl. Data Tables* **1974**, *14*, 177.
(21) Basch, H.; Gray, H. B. *Theor. Chim. Acta* **1966**, *4*, 367.

Table 4. Parameters for EH Calculations

	orbital	H_{ii}, eV	$\zeta_1{}^b$	$\zeta_2{}^b$	$c_1{}^a$	$c_2{}^a$
Nb	4d	−9.94	4.08	1.640	0.6401	0.5516
	5s	−9.04	1.89			
	5p	−5.15	1.85			
P	3s	−18.6	1.88			
	3p	−12.5	1.63			

[a] Coefficients used in double-ζ expansion. [b] Slater-type orbital exponents.

Appendix

All calculations employed the extended Hückel (tight-binding) method[18,19] (parameters appear in Table 4). Exponents were taken from standard sources.[20,21] Valence state ionization energies (H_{ii}'s) for Nb were obtained from a charge iterative calculation on NbP. The DOS curves in Figure 5a,b entailed the use of 165K points in the irreducible wedge of the primitive tetragonal Brillouin zone. For the calculation of three-center-bonding orbital projection (Figure 5c), we found it convenient to quadruple the size of the unit cell so that entire Nb_3 triangles were contained within it. With this expanded cell, we performed a calculation using 20K points in the irreducible wedge of the primitive tetragonal Brillouin zone.

Supporting Information Available: Tables giving X-ray crystallographic details (Table SI), interatomic distances and angles (Table SII), and anisotropic displacement parameters (Table SIII) (5 pages). Ordering information is given on any current masthead page.

IC950826F